

# Estimating Large-Scale Network Convergence in the Human Functional Connectome

Peter T. Bell<sup>1</sup> and James M. Shine<sup>1,2</sup>

## Abstract

The study of resting-state networks provides an informative paradigm for understanding the functional architecture of the human brain. Although investigating specialized resting-state networks has led to significant advances in our understanding of brain organization, the manner in which information is integrated across these networks remains unclear. Here, we have developed and validated a data-driven methodology for describing the topography of resting-state network convergence in the human brain. Our results demonstrate the importance of an ensemble of cortical and subcortical regions in supporting the convergence of multiple resting-state networks, including the rostral anterior cingulate, precuneus, posterior cingulate cortex, posterior parietal cortex, dorsal prefrontal cortex, along with the caudate head, anterior claustrum, and posterior thalamus. In addition, we have demonstrated a significant correlation between voxel-wise network convergence and global brain connectivity, emphasizing the importance of resting-state network convergence in facilitating global brain communication. Finally, we examined the convergence of systems within each of the individual resting-state networks in the brain, revealing the heterogeneity by which individual resting-state networks balance the competing demands of specialized processing against the integration of information. Together, our results suggest that the convergence of resting-state networks represents an important organizational principle underpinning systems-level integration in the human brain.

**Key words:** connectivity; cortex; integration; network; resting-state; segregation; subcortex

## Introduction

RECENT TECHNOLOGICAL and conceptual advances in Systems Neuroscience have led to sophisticated descriptions of the connectional organization of the human brain (Sporns, 2011). At the macroscopic scale, the human brain is organized into large-scale networks. Although these networks were originally discovered during analysis of the “resting” brain (Beckmann et al., 2005), similar patterns of coordinated activity are also consistently detected across a wide variety of task domains (Cole et al., 2014; Laird et al., 2013; Smith et al., 2009), suggesting that the investigation of resting-state networks can provide fundamental insights into the functional architecture of the human brain (Buckner et al., 2013).

The neuronal networks that comprise the human brain share a number of connectional properties that minimize energy requirements and maximize the ability to broadcast information (Bullmore and Sporns, 2009). Indeed, specialization within modular networks alone cannot support global cognitive func-

tion and must be balanced against the competing processing requirement to integrate and unite this information to support coherent cognitive operations (Fox and Friston, 2012; Tononi et al., 1994). Although mechanisms underpinning neural integration are currently an area of investigation (Sporns, 2013), it is not yet clear how specialized neural systems integrate and disseminate information.

Several neuroimaging studies have begun to characterize neural regions that are likely to participate in multiple resting-state networks (Braga et al., 2013; Leech et al., 2011; Power et al., 2013; van den Heuvel and Sporns, 2013; Yeo et al., 2013), offering novel insights into how neural signals might be integrated across specialized modules in the human brain. Pioneering graph analytic work by van den Heuvel and Sporns (2013) employed a combination of high-resolution structural tractography and resting-state functional magnetic resonance imaging (fMRI) to demonstrate that an anatomical core of highly central, densely interconnected, and metabolically expensive neural regions—the so-called “rich-club”—is likely implicated in the integration of information across

<sup>1</sup>Brain and Mind Research Institute, The University of Sydney, Camperdown, New South Wales, Australia.

<sup>2</sup>Department of Psychology, Stanford University, Stanford, California.

resting-state networks. In addition, several other recent studies have begun to emerge (Braga et al., 2013; Power et al., 2013; Yeo et al., 2013), providing an initial glimpse into the possible candidate architecture involved in systems-level integration in the brain.

Although the results from this recent work support the importance of an assembly of interconnected neural regions in systems-level integration, there remains ongoing debate regarding the precise neuronal architecture involved in inter-modular communication [e.g., see Power et al. (2013) and Warren et al. (2014)] and how this architecture might contribute to the global brain communication. In addition, the contribution of subcortical structures in large-scale network communication has been relatively poorly described to date. Furthermore, although recent studies have implicated several candidate regions in resting-state network communication (Braga et al., 2013; Power et al., 2013; van den Heuvel and Sporns, 2013; Yeo et al., 2013), the extent and heterogeneity of large-scale network convergence across the topography of the cerebrum is not yet clear.

The motivations behind this study were threefold: (1) to develop a new method for estimating the functional architecture involved in systems-level integration [to complement existing graph analytic descriptions of multiple-network participation, e.g., Power et al. (2013)]; (2) to characterize large-scale network convergence in subcortical structures including the basal ganglia, thalamus, and cerebellum; and (3) to further describe the extent and heterogeneity of multiple-network membership across the topography of the brain. To achieve these aims, we have developed and validated a methodology for investigating patterns of large-scale network convergence across the topography of cortical and subcortical structures. In addition to whole-brain descriptions of network convergence, we also provide a series of novel convergence maps that characterize the topography of network convergence within each of the individual cortical and subcortical networks, offering new perspectives regarding the topography by which individual networks differentially balance the competing demands of specialized processing against integration of information across networks.

## Methods

### Overview

The overarching goal of this experiment was to characterize the topographic architecture supporting large-scale network convergence in the human brain. To achieve this aim, we utilized a combination of spatial independent component analysis (ICA) and a graph theoretical connectivity measure to explore patterns of large-scale network convergence.

### Image acquisition and preprocessing

Data from 100 healthy adults (mean age = 21.4 years; 63% female) were obtained from the Cambridge dataset in the 1000 Functional Connectomes data repository (Biswal et al., 2010). Imaging was conducted on a General Electric 3T MRI (General Electric). T2\*-weighted echo planar functional images were acquired in sequential order with repetition time = 3000 msec, echo time = 32 msec, flip angle = 90°, 47 axial slices covering the whole brain, field of view = 220 mm, and raw voxel size = 3 × 3 × 3 mm thick, 119 TRs (scan

time = 420 sec). High-resolution 3D T1-weighted, anatomical images (voxel size 1.2 mm isotropic) were obtained for co-registration with functional data. Resting-state functional images were collected on participants with their eyes closed.

Statistical parametric mapping software (SPM8) was used for image preprocessing, according to a standard pipeline: (1) scans were slice-time corrected to the median (21st) slice in each repetition time; (2) scans were then realigned to create a mean realigned image while estimates of six degrees of head movement were calculated for later use; (3) a 7th-degree B-spline was used for interpolation; (4) images were normalized to the echo planar image template; and (5) scans were then smoothed using an 8-mm full-width at half maximum isotropic Gaussian kernel.

### Spatial ICA

Preprocessed images were subjected to two separate group-level spatial ICA using the GIFT toolbox (Calhoun et al., 2001) in SPM8, one for the Discovery sample ( $n=50$ ), and one for the Replication sample ( $n=50$ ). Briefly, spatial ICA is a data-driven approach that searches for maximally independent clusters of voxels within the brain that co-vary together in reliable temporal relationships (Calhoun et al., 2001). Using the GIFT toolbox, this process involves data reduction using principle component analysis, followed by spatial ICA and finally, a back projection step to re-create individual subject maps for each component (Calhoun et al., 2001).

The Discovery cohort and the Replication cohort were analyzed separately using the InfoMax algorithm in the GIFT toolbox (Calhoun et al., 2001). In both the Discovery cohort and the Replication cohort, the minimum description length criterion was used to estimate the number of independent components, and it was found to be 16 in both groups. For both the Discovery and Replication cohort datasets, the 16 components were then examined for the presence of artifactual noise (i.e., spatial patterns associated with the ventricular system, white matter, or the edges of the brain). In both the Discovery cohort and the Replication cohort, a total of three artifactual components were identified and thus discarded from further analysis. Therefore, 13 nonartifactual independent components were identified in both the Discovery cohort (Fig. 1) and the Replication cohort, the number of which is consistent with findings from fully exploratory ICA in 1000 individuals (Kalcher et al., 2012).

The components identified in this study were the Sensorimotor component (SM), Visual component (VIS), Temporal lobe component (TEMP), Thalamic component (THAL), Brainstem component (BS), Basal Ganglia component (BGN), Cerebellar component (CBM), Left (LFPN) and Right (RFPN) Lateralized Frontoparietal Network components, Ventral Attention Network component (VAN), Dorsal Attention Network component (DAN), Precuneus component (PCU), and Default Mode Network component (DMN). See Fig. 1 for visualization of the group-level network components extracted in the Discovery cohort. Importantly, the spatial components extracted from the Discovery cohort and the Replication cohort showed strong spatial overlap (Pearson's  $r > 0.500$ ,  $p < 0.001$  for each component comparison). In addition, for each component, spatial sorting using the component defined in the Discovery group reliably

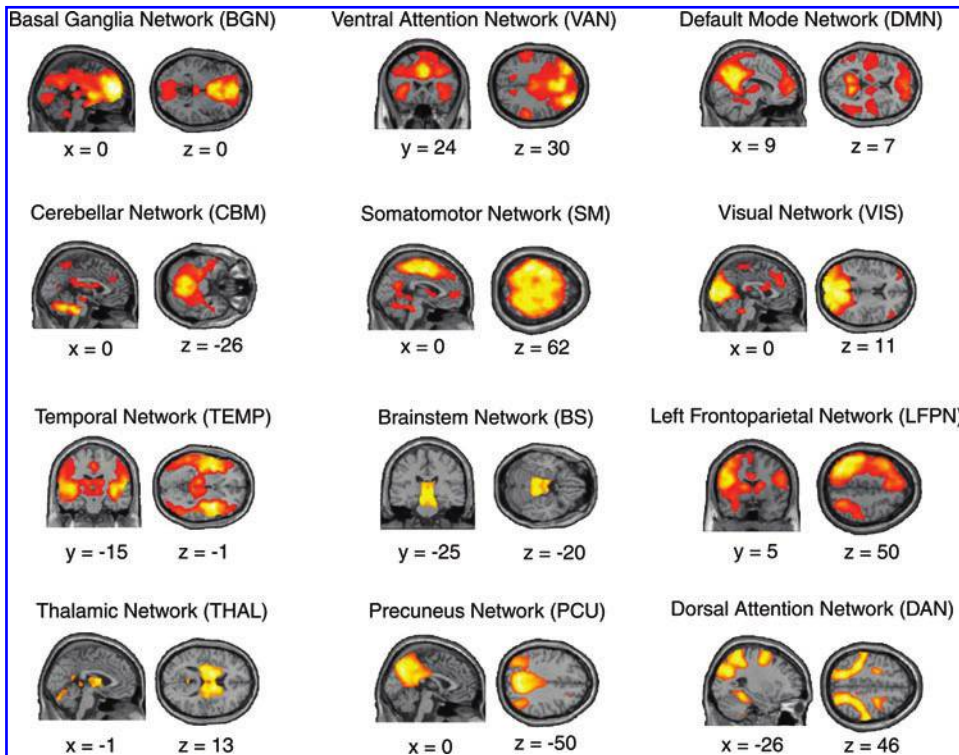


**FIG. 1.** Spatial independent components. Group-level network maps of 12 independent components extracted using spatial independent component analysis. Each component was labeled according to either its known nomenclature (e.g., DMN) or to its most prominent neuroanatomical feature (e.g., thalamus or temporal lobe). Data shown for the Discovery cohort when spatial components were thresholded at  $p < 0.001$ ; FDR  $p = 0.01$ . Note that, for ease of visualization the Right Frontoparietal Network is not shown here. DMN, Default Mode Network; FDR, false detection rate. Color images available online at [www.liebertpub.com/brain](http://www.liebertpub.com/brain)

identified the corresponding spatial component in the Replication group.

#### Estimation of resting-state network convergence

The subsequent analyses were applied to both the Discovery cohort and the Replication cohort separately (see Supplementary Methods: Reproducibility of estimates of network convergence in an independent Replication cohort; Supplementary Data are available online at [www.liebertpub.com/brain](http://www.liebertpub.com/brain)). Spatial maps representing each of the 13 non-artifactual components for each individual subject were entered into separate random effects analyses (one for each component) at the group-level using SPM8 software. These group-level spatial maps were then thresholded statistically at  $p < 0.001$  (corrected for multiple comparisons using a false detection rate [FDR] of  $p = 0.01$ ), leading to the extraction of a binary mask for each of the 13 network components, respectively. After extracting only voxels that existed with a standard gray matter mask from the WFU Pick Atlas toolbox (Maldjian et al., 2003), we created a novel spatial convergence map by amalgamating each of these 13 binary component maps together in the same topographic space, allowing the calculation of a *network convergence metric* (NCM) at each voxel of the brain (Eq. 1). As such, the NCM calculated at each individual voxel in the group-level convergence map represents the number of maximally independent resting-state networks that converge at the specific brain voxel. Importantly, given that spatial ICA maximizes the spatial independence between independent components, patterns of spatial overlap between resting-state networks may actually be more extensive than described here (see Discussion: The role of whole-brain network convergence in global brain communication, for further discussion addressing this topic).

$$\text{NCM}_x = \sum(\text{IC}_x) \quad \text{Eq. 1}$$

The NCM was defined as the sum of independent components at a given voxel ( $x$ ) that were present above chance after spatial ICA ( $p < 0.001$ ; FDR  $p = 0.01$ ).

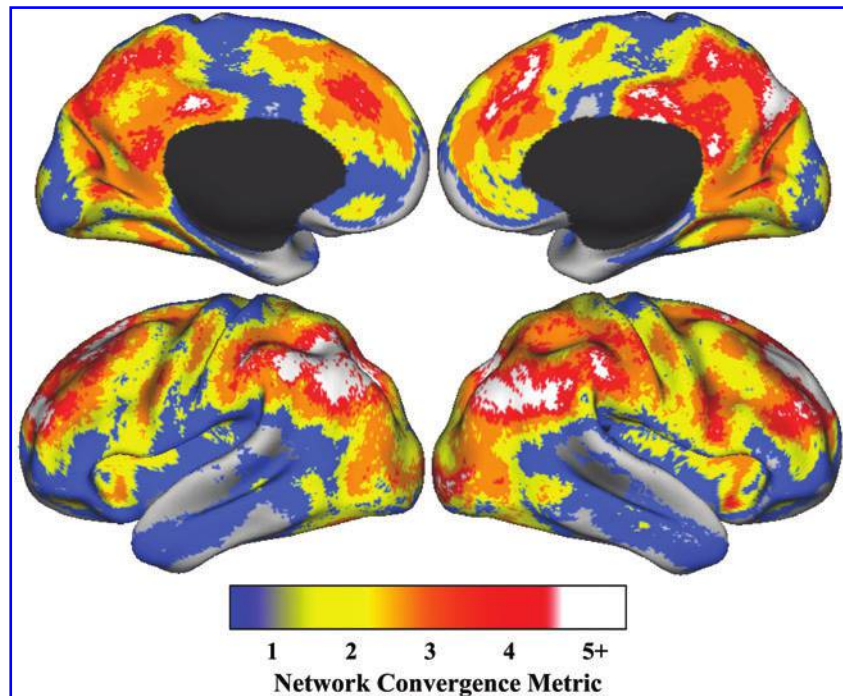
#### Relationship between network convergence and global connectivity

In this analysis, we sought to examine whether network convergence was related global brain connectivity (as calculated using an independent graph-theoretical metric, see below). A relationship between the NCM and global brain connectivity would support the hypothesis that large-scale network convergence facilitates efficient global brain communication. To explore this hypothesis we extracted a previously described graph theoretic connectivity measure, the Intrinsic Connectivity Contrast (ICC) (Martuzzi et al., 2011), from every voxel in the brain. Briefly, the ICC reflects the sum of the correlation of each source voxel to every other voxel in the brain, which is then weighted by the  $R^2$  value associated with the voxel-to-voxel connection (Martuzzi et al., 2011). Note that the ICC analysis was conducted on the same resting-state fMRI dataset, however, before spatial smoothing (Martuzzi et al., 2011). We then correlated the voxel-wise ICC score with the NCM using Spearman's rank-order correlation coefficient.

#### Convergence within individual resting-state networks

In addition to providing spatial descriptions of resting-state network convergence across the entire brain (Figs. 2 and 3), we also estimated patterns of network convergence *within* individual networks (Fig. 4). To achieve this, we created 13 separate spatial convergence maps, in which each of

**FIG. 2.** Topography of network convergence across the cerebral cortex. Spatial convergence map depicting the number of maximally independent resting-state networks that converge at each cortical voxel (NCM). Color spectrum denotes the voxel-wise NCM: gray—regions that were not covered by any of the 13 large-scale networks; blue—voxels associated with only one large-scale network; yellow—voxels associated with convergence of two networks; orange—voxels associated with convergence of three networks; red—voxels associated with convergence of four networks; white—voxels associated with convergence of five or more networks. Data shown for the Discovery cohort when spatial components were thresholded at  $p < 0.001$ , FDR  $p = 0.01$ . NCM, network convergence metric. Color images available online at [www.liebertpub.com/brain](http://www.liebertpub.com/brain)



the network masks identified in the original spatial ICA (see Methods: Spatial ICA) were individually defined as a *host* network mask (thresholded at  $p < 0.001$ , FDR  $p = 0.01$ ). The extent of network convergence at every voxel within the *host* network was estimated by calculating the NCM (as per Methods: Estimation of resting-state network conver-

gence) exclusively for voxels that were within the topography of the host network mask, creating estimates of network convergence *within* the topography of large-scale networks of the brain.

To calculate the relative balance of each network toward integrative or segregative processing, we calculated the proportion of the total host network voxels that were significantly involved in network convergence (Network Convergence Ratio [NCR]). Importantly, the spatial extent of network component maps derived from spatial ICA is somewhat contingent on the particular statistical threshold applied to the data, with more stringent thresholds associated with less expansive spatial components and vice versa [see Supplementary Results: Reproducibility over multiple statistical thresholds and Calhoun et al. (2001)]. To circumvent this potential issue, we calculated a *threshold-adjusted Z-score* at each brain voxel (see Supplementary Methods: Reproducibility over multiple statistical thresholds, for further methodological detail), which accounted for variability in voxel-wise network convergence patterns across a wide range of component thresholds (thresholds ranging from  $p = 1 \times 10^{-1}$  to  $1 \times 10^{-10}$ ).

The NCR was subsequently characterized for each component by calculating the proportion of the total *host* voxels that were significantly involved in network convergence, controlling for variability across different component thresholds (mean *threshold-adjusted Z-score*:  $Z > 1.65$ ,  $p < 0.05$ ). The NCR for each host network was then plotted onto a radar plot (Fig. 5), enabling a qualitative description of the heterogeneity by which different individual networks differentially balance the competing demands of specialized processing against integration of information across networks. This analysis was also repeated with a more stringent *threshold-adjusted Z-score* threshold ( $Z > 2.33$ ,  $p < 0.01$ ) to ensure these results were robust to the significance threshold applied.

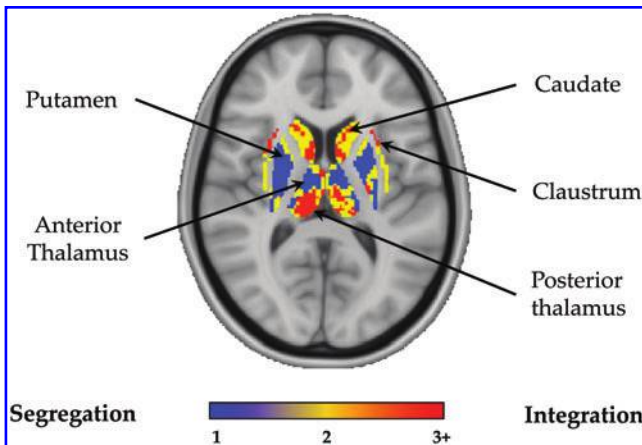


**FIG. 3.** Topography of network convergence across the basal ganglia and thalamus. Subcortical slice through the basal ganglia and thalamus ( $x = -4$ ,  $y = -20$ ) depicting the number of maximally independent resting-state networks that converge at each subcortical voxel (NCM). Color spectrum denotes the voxel-wise NCM; blue—voxels associated within only one network; yellow—voxels associated with convergence between two networks; red—voxels associated with convergence between three or greater networks; gray—regions that were not covered by any of the 13 large-scale networks. Data shown for the Discovery cohort when spatial components were thresholded at  $p < 0.001$ , FDR  $p = 0.01$ . Color images available online at [www.liebertpub.com/brain](http://www.liebertpub.com/brain)

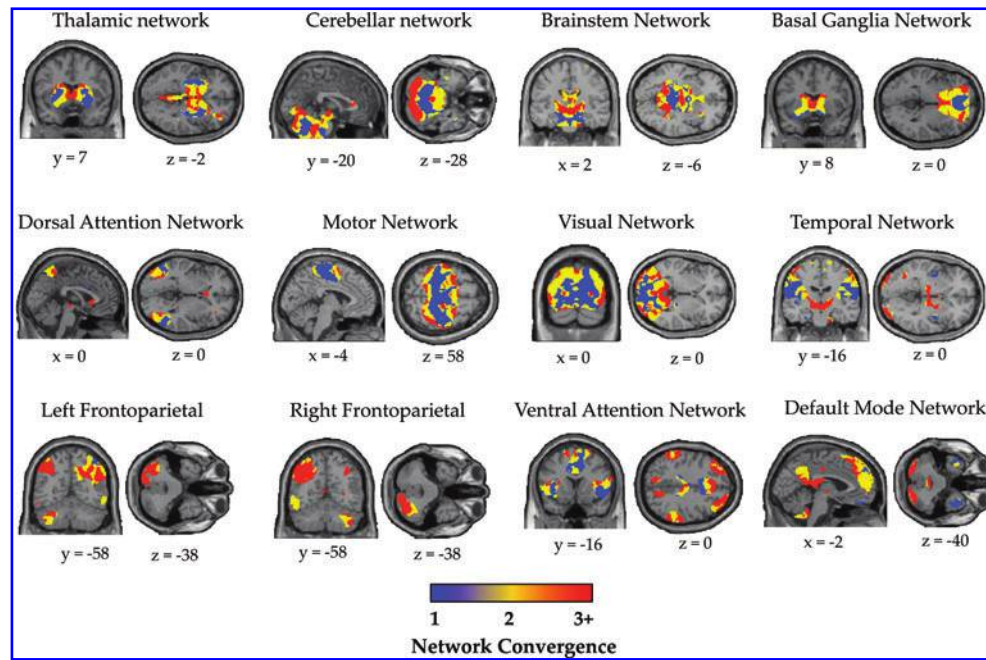


**FIG. 4.** Convergence within individual network components. Brain slices depicting the number of neuronal networks that are shared at each voxel (NCM) within each of the individual large-scale networks of the brain. For each network component, the color spectrum denotes the extent that a given voxel was shared with the other networks of the brain: blue—voxels that participate only in the host network; yellow—voxels associated with convergence of two networks; red—voxels associated with convergence between three or greater networks; gray—voxels that were outside of the network component mask. Data shown for the Discovery cohort when spatial components were thresholded at  $p < 0.001$ , FDR  $p = 0.01$ . For clarity, PCU component not shown. PCU, Precuneus component; NCM, Network Convergence Metric. Color images available online at [www.liebertpub.com/brain](http://www.liebertpub.com/brain)

Of note, both the BGN and THAL components derived from the group-level spatial ICA were also associated with a number of cortical voxels (Fig. 1). Therefore, convergence patterns within the BGN and THAL host networks may have been influenced by the connectional properties of their respective cortical associations. In this analysis, we were interested in describing the integrative properties—not only within the broader THAL and BGN networks in the context of their cortical associations (Fig. 1) but also within the distinct anatomical boundaries of these subcortical structures. Therefore, we also calculated the NCR within anatomically defined gray matter masks exclusively encompassing voxels within the basal ganglia (BGN<sub>anat</sub>) and thalamus (THAL<sub>anat</sub>), respectively (Fig. 5).

#### Validation analyses

Finally, we conducted an extensive series of validation analyses to ensure the robustness of our methodology. The methods for these validation analyses are described in detail in the Supplementary Methods section. Specifically, we conducted validation analyses to demonstrate that our estimates of network convergence were (1) reproducible in an independent Replication cohort (Supplementary Methods: Reproducibility of estimates of network convergence in an independent Replication cohort); (2) robust to the methodology used to define the topography of spatial networks (Supplementary Methods: Reproducibility using seed-based connectivity to define large-scale networks); (3) robust to the number of independent components defined (Supplementary Methods: Reproducibility of whole-brain network con-

vergence with variable number of network components); (4) robust to variable statistical thresholding (Supplementary Methods: Reproducibility over multiple statistical thresholds); and (5) reproducible at the individual subject level (Supplementary Methods: Reproducibility of whole-brain network convergence at the individual subject level).

#### Data visualization

For group-level interpretation, data were displayed on the lateral and medial surfaces of a partially inflated surface map using CARET software (Van Essen et al., 2001), allowing the projection of a series of qualitative topographic descriptions of network convergence in the brain. These spatial convergence maps enable the graphical interrogation of the voxel-wise NCM at a statistical threshold commonly reported in the literature ( $p < 0.001$ , FDR  $p = 0.01$ ; Fig. 2). Note that, for ease of visualization and data interpretation we opted to parcellate the network convergence maps into three “levels” when displaying data for the subcortical convergence map (Fig. 3) and within-network convergence maps (Fig. 4). Importantly, parcellation into levels (Figs. 3 and 4) was purely for the purposes of visualization, and all statistical analyses were conducted on the unparcellated NCM (as displayed in Fig. 1). The rationale for parcellating data into three levels was based on the observation that, at a statistical threshold of  $p < 0.001$ , FDR  $p = 0.01$ , approximately one-third of voxels revealed convergence of one (36.8%), two (39.3%), or ≥three (23.9%) networks respectively, enabling a clear and easily interpretable schema for data visualization.

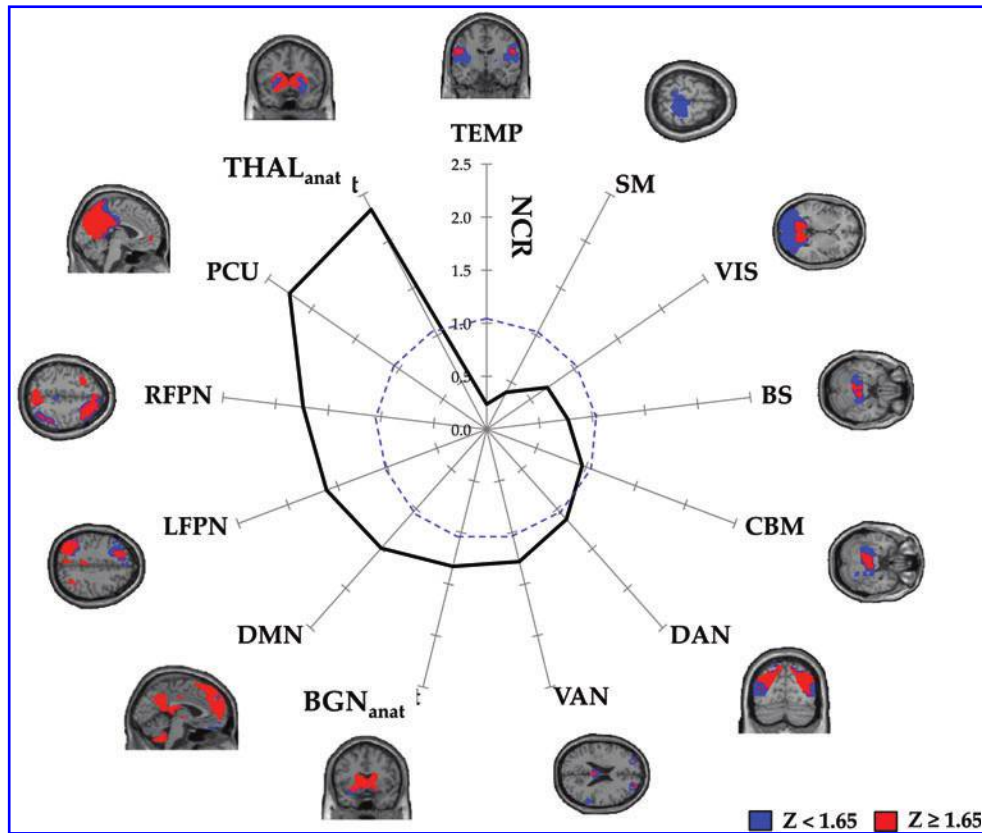


**FIG. 5.** Heterogeneity of network convergence across individual large-scale networks. Radar plot revealing the NCR for each individual large-scale network, calculated as the proportion of voxels in each individual network mask that were consistently associated with high-order convergence across a range of statistical thresholds. NCR = 1.0 is denoted by a dashed blue line. Spatial maps represent binarized threshold-adjusted convergence maps within each of the individual large-scale networks, revealing regions consistently involved in high-order network convergence across a range of statistical thresholds (red) relative to all other brain voxels (blue). BGN<sub>anat</sub>, Basal Ganglia Nuclei (anatomical mask); BS, Brainstem component; CBM, Cerebellar component; DAN, Dorsal Attention Network component; DMN, Default Mode Network component; LFPN, Left Frontoparietal Network component; NCR, Network Convergence Ratio; RFPN, Right Frontoparietal Network component; SM, Sensorimotor Network component; TEMP, Temporal Lobe component; THAL<sub>anat</sub>, Thalamic nuclei (anatomical mask); VAN, Ventral Attention Network component; VIS, Visual component. Color images available online at [www.liebertpub.com/brain](http://www.liebertpub.com/brain)

## Results

### *Estimation of network convergence at the level of the whole-brain*

The 13 resting-state networks of interest covered 94.6% of the total brain gray matter volume—encompassing almost the entire brain, except for clusters within the orbitofrontal cortex, mid-cingulate, and lateral temporal cortex (Fig. 2; statistical threshold;  $p < 0.001$ , FDR  $p = 0.01$ ). We observed marked heterogeneity in the propensity for resting-state network convergence across the brain. 31.8% of voxels within the gray matter mask were associated with only one resting-state network (Figs. 2 and 3—blue and Table 1), which predominantly occurred in the bilateral primary motor cortex, bilateral primary visual cortex, pons, putamen, anterior thalamus, lateral orbitofrontal cortex, temporal poles, and lobule IV/V of the cerebellum (Table 1). 30.1% of voxels were shared between two resting-state networks (Figs. 2 and 3—yellow and

Table 1), including predominant regions within the middle cingulate, cuneus, bilateral premotor areas, medial orbitofrontal cortex, posterior claustrum, and lobule VI of the cerebellar cortex. The remaining 38.1% of voxels supported the convergence of three or greater resting-state networks. Regions supporting convergence across three resting-state networks included midline frontal pole, bilateral inferior frontal gyri, midbrain, and Crus I of the cerebellum (Fig. 2—orange and Table 1). Regions demonstrating convergence across four networks included the pre-supplementary motor areas, posterior cingulate cortex, medial prefrontal cortex, and superior parietal lobule, along with the head of the caudate nucleus, anterior claustrum, posterior thalamus, and bilateral Crus II of the cerebellum (Fig. 2—red and Table 1). Finally, neural regions supporting convergence across five networks included the midline rostral anterior cingulate and precuneus, bilateral posterior parietal cortex and the bilateral superior, and middle frontal gyri (Fig. 2—white and Table 1).

TABLE 1. LARGE-SCALE NETWORK CONVERGENCE

Network convergence	Hemisphere	Neural region	Coordinates		
			x	y	z
≥5	Mid	rACC	0	38	35
	Mid	PCu	0	-40	35
	BL	PPC	±47	-80	36
	BL	SFG	±22	15	45
	BL	MFG	±34	58	16
4	Mid	pSMA	0	23	44
	Mid	PCC	0	-36	34
	Mid	mPFC	0	52	12
	BL	SPL	±44	-62	46
	BL	Crus II	±33	-75	-42
	BL	Caudate head	±7	16	0
	BL	Post thalamus	±8	-24	13
3	BL	Ant claustrum	±36	9	0
	Mid	FP	0	59	-5
	BL	Midbrain	±7	-14	-8
	BL	Crus I	±34	-63	-33
	BL	IFG	±20	56	2
2	Mid	MCC	0	22	30
	Mid	Cuneus	0	-82	30
	Mid	Medial OFC	0	23	-13
	BL	Med thalamus	±14	-18	1
	BL	PMA	±26	2	60
	BL	Lobule VI	±26	-76	-18
1	BL	Post claustrum	±38	5	-10
	BL	Lateral OFC	±10	35	-16
	BL	M1	±24	-29	62
	BL	V1	±14	-94	9
	BL	Ant thalamus	±12	-3	0
	BL	Putamen	±22	-7	6
	BL	Pons	±2	-30	-34
	BL	TempP	±47	0	-34
BL	Lobule IV/V	±9	-55	-18	

Ant, anterior; BL, bilateral; Crus, cerebellar crus; FP, frontal pole; IFG, inferior frontal gyrus; Lobule, cerebellar lobule; M1, primary motor cortex; MCC, middle cingulate gyrus; MFG, middle frontal gyrus; Mid, midline; mPFC, medial prefrontal cortex; OFC, orbito-frontal gyrus; PCC, posterior cingulate cortex; Post, posterior; PCu, precuneus; PMA, premotor area; PPC, posterior parietal cortex; pSMA, presupplementary motor area; rACC, rostral anterior cingulate cortex; SFG, superior frontal gyrus; SPL, superior parietal lobule; TempP, temporal pole; V1, primary visual cortex.

#### Relationship between network convergence and global connectivity

To examine whether network convergence was related to an independent graph-theoretic measure of global brain connectivity we correlated the NCM with ICC. We found a significant positive correlation between the NCM and ICC ( $\rho=0.543$ ,  $p<0.001$ ), suggesting that the number of resting-state networks that converge on a given voxel was related to the global connectedness of the voxel within the context of the whole-brain.

#### Convergence within individual networks

We have provided novel spatial maps describing the topography of network convergence within each of the 13 components extracted from the spatial ICA (Fig. 4). We observed substantial heterogeneity in the convergence patterns

within individual resting-state networks (Figs. 4 and 5). This heterogeneity was further illustrated by plotting the NCR for each individual resting-state network (Fig. 5). The NCR radar plot (Fig. 5) demonstrates that associative networks, along with the thalamus and basal ganglia are qualitatively balanced toward integrative processing, whereas sensorimotor, visual, brainstem, and temporal networks are balanced toward segregated processing.

#### Validation analyses

In a series of validation analyses we have shown that our estimates of network convergence are (1) reproducible in an independent Replication cohort (Supplementary Results: Reproducible estimates of network convergence in an independent Replication cohort; Supplementary Fig. S1A); (2) robust to the methodology used to define the topography of spatial networks (Supplementary Results: Reproducibility using seed-based connectivity to define resting-state networks); (3) robust to the number of independent components defined (Supplementary Results: Reproducibility of whole-brain network convergence with variable number of network components); (4) robust to variable statistical thresholding (Supplementary Results: Reproducibility over multiple statistical thresholds; Supplementary Fig. S1B); and (5) reproducible at the individual subject level (Supplementary Results: Reproducibility of network convergence at the individual subject level).

#### Discussion

In this article, we developed a data-driven methodology for describing the topography of resting-state network convergence in the human brain (Figs. 2 and 3). In addition, we have demonstrated a significant relationship between whole-brain network convergence and global brain connectivity at the level of the individual voxel, emphasizing the importance of large-scale network convergence in supporting global communication in the human brain. Furthermore, we examined the convergence of systems within each of the individual large-scale networks of the brain (Figs. 4 and 5), offering new perspectives regarding the topography by which individual networks differentially balance the competing demands of specialized processing against the integration of information. Importantly, we provided extensive validation of our methodology by demonstrating that our estimates of network convergence were (1) reproducible in an independent cohort (Supplementary Results: Reproducible estimates of network convergence in an independent Replication cohort; Supplementary Fig. S1); (2) robust to the methodology used to define the topography of spatial networks (Supplementary Results: Reproducibility using seed-based connectivity to define resting-state networks); (3) robust to the number of independent components defined (Supplementary Results: Reproducibility of whole-brain network convergence with variable number of network components; Supplementary Fig. S1B); (4) robust to variable statistical thresholding (Supplementary Results: Reproducibility over multiple statistical thresholds); and (5) reproducible at the individual subject level (Supplementary Results: Reproducibility of network convergence at the individual subject level).

*The role of whole-brain network convergence in global brain communication*

The results of our analyses revealed an ensemble of neural regions involved in the convergence of multiple resting-state networks, consisting of neural regions including the rostral anterior cingulate, precuneus, posterior cingulate cortex, posterior parietal cortex, dorsal prefrontal cortex, superior parietal lobule, along with the head of the caudate nucleus, anterior claustrum, and posterior thalamus. The cortical regions implicated in high-level network convergence in this study are broadly consistent with findings from initial studies that have begun to characterize regions that are likely to support inter-modular communication in the brain. Together, converging evidence from this (Figs. 2 and 3) and other work (Braga et al., 2013; Power et al., 2013; van den Heuvel and Sporns, 2013; Yeo et al., 2011), suggests that a core backbone of cortical hubs including the posterior cingulate/precuneus (Braga et al., 2013; van den Heuvel and Sporns, 2013; Yeo et al., 2013), anterior cingulate (Braga et al., 2013) along with posterior parietal (van den Heuvel and Sporns, 2013; Yeo et al., 2013) and prefrontal regions (Power et al., 2013; van den Heuvel and Sporns, 2013; Yeo et al., 2013), are important for the integration of information across specialized brain networks. Therefore, our findings provide complementary evidence—utilizing a novel methodology—to support the functional importance of a core backbone of neural regions in inter-network integration in the brain (Sporns, 2013). Furthermore, in this study we have characterized patterns of network convergence in the human subcortex (Fig. 3), which have not been described in previous work. Specifically, we demonstrate the involvement of the caudate head, anterior claustrum, and posterior thalamus (Fig. 3) in systems-level integration in the brain.

Broadly, our findings suggest that at the macroscale, areas of network convergence contain an amalgamation of neural signals that can be decomposed into a series of overlapping constituent network components using both multivariate (Figs. 2 and 3) [also see Braga et al. (2013), Geranmayeh et al. (2014), Yeo et al., (2013)] and univariate (see Supplementary Results: Reproducibility using seed-based connectivity to define resting-state networks) approaches. These findings are consistent with the prediction that transmodal regions will contain amalgamated neural signals that partially correlate with signals arising from their input networks (Mesulam, 1998). Despite these insights, local circuit mechanisms that coordinate the dynamic integration of incoming neural signals remain unclear (Braga and Leech, 2015).

In this work we have also demonstrated a direct relationship between network convergence and an independent graph theoretical measure of global brain connectivity, further emphasizing the importance of large-scale network convergence in efficient global brain communication (van den Heuvel and Sporns, 2013). A recent study comparing various graph analytic metrics that describe aspects of network centrality, revealed the non-redundancy of different centrality measures in resting-state brain networks (Zuo et al., 2012). Therefore, although we demonstrate a significant positive correlation between network convergence and global brain connectivity as defined by ICC [a weighted measure of degree centrality at the level of the individual voxel Martuzzi et al. (2011)], it is likely that these metrics are measuring subtly

different, although inter-related, properties of the brain graph. For example, the graph-analytic literature has identified two broad categories of brain hubs: “connector” and “provincial” hubs (Sporns et al., 2007). Connector hubs are high-degree nodes with connectivity profiles that expedite communication across different network communities, whereas provincial hubs are high-degree nodes with dense connections to other nodes within their own community. Degree-based methods are unable to effectively distinguish between provincial and connector nodes (Sporns et al., 2007), which may explain one way in which the inter-related measures of network convergence and ICC differ. Although not the focus on this study, future work will help to further clarify the precise inter-relationships between various graph analytic measures of centrality and network convergence.

*Insights into the extent of network convergence in the brain*

The methodological use of spatial ICA to define large-scale resting-state networks in this study provides insights into the extent and heterogeneity of resting-state network convergence in the brain. Importantly, despite the definition of network components using spatial ICA, which is designed to maximize spatial independence between individual network components (Calhoun et al., 2001), we still found substantial network convergence across both the cortex and subcortex across a range of statistical thresholds used to define the network components (Supplementary Results: Reproducibility over multiple statistical thresholds). Such extensive spatial overlap across network components, despite the use of a method designed to maximize spatial independence, has implications for the interpretation of neuroimaging data and the way in which brain parcellation is conceptualized. In particular, these findings emphasize the importance of recognizing the limitations of many existing parcellation strategies that unrealistically assume that any given neural region cannot simultaneously belong to two or more different modules [see Papo et al. (2014) for further discussion].

*Heterogeneity of convergence within individual large-scale networks*

In addition to whole-brain descriptions of network convergence, we also characterize the spatial patterns of network convergence *within* individual large-scale networks (Figs. 4 and 5), which to our knowledge, have not been previously described. We utilized estimates of network convergence to show that, although each large-scale network demonstrates the dual organizational properties of integration and segregation, there is marked heterogeneity in the way in which individual networks balance these competing organizational properties (Figs. 4 and 5). Specifically, we have shown that putative association networks, including the DMN, bilateral FPNs, DAN, and VAN, along with the basal ganglia and thalamus are differentially balanced toward integrative information processing (Fig. 5). In stark contrast, unimodal networks including the visual and sensorimotor networks, along with the temporal and brainstem networks are balanced toward segregative processing (Fig. 5). These results are aligned with the notion that association networks participate in long-distance (Sepulcre et al., 2010), flexible (Cole et al., 2013), dynamic (Zalesky et al., 2014), and globally connected (Buckner et al., 2009; Cole

et al., 2010; van den Heuvel and Sporns, 2013) information processing in the brain, and suggest that association networks may play a central role in facilitating the integration of information across distributed cortical regions (Yeo et al., 2013).

Furthermore, our data provide novel evidence to suggest that subcortical structures such as the basal ganglia and the thalamus also support integration across large-scale networks of the brain (Figs. 3–5). Although these subcortical structures have classically been viewed as mere relay stations for parallel processing within functionally segregated cortical-subcortical loops (Alexander et al., 1986), an emerging body of neuroanatomical data has identified pathways for communication across functional subdivisions of the basal ganglia (Averbeck et al., 2014; Haber, 2008) and the thalamus (Draganski et al., 2008), suggesting that the subcortex may provide an important and relatively unexplored nexus for the integration of neural signals across modular neural systems. Future work exploring the integrative capacities of the often-neglected subcortical nuclei (Parvizi, 2009) presents an exciting avenue for future discovery.

In this study we examined the topography of time-averaged resting-state networks. However, emerging work has begun to suggest that functional connectivity may be variable over time (Hutchison et al., 2013). Although there are a number of technical challenges facing the study of time-resolved connectivity analyses (Zalesky and Breakspear, 2015), future work examining how functional networks transiently coalesce at finer temporal scales will further clarify how information is dynamically integrated across large-scale neural systems.

## Conclusion

Characterizing neuronal network convergence at the macro-scale is fundamental in understanding global brain function. In this study, we estimate the topography of resting-state network convergence across the whole brain and within individual networks, offering new insights into the complex functional architecture of the human brain. Our results shed new light on how information might propagate throughout cortical and subcortical brain networks.

## Acknowledgments

We would like to thank Michael Hornberger and Claire O'Callaghan for their critical review of the article. We would also like to thank the organizers of the 1000 Functional Connectomes Project for sharing the data used in the study.

## Author Disclosure Statement

No competing financial interests exist.

## References

- Alexander GE, DeLong MR, Strick PL. 1986. Parallel organization of functionally segregated circuits linking basal ganglia and cortex. *Annu Rev Neurosci* 9:357–381.
- Averbeck BB, Lehman J, Jacobson M, Haber SN. 2014. Estimates of projection overlap and zones of convergence within frontal-striatal circuits. *J Neurosci* 34:9497–9505.
- Beckmann CF, DeLuca M, Devlin JT, Smith SM. 2005. Investigations into resting-state connectivity using independent component analysis. *Philos Trans R Soc B Biol Sci* 360:1001–1013.
- Biswal BB, Mennes M, Zuo X-N, Gohel S, Kelly C, Smith SM, Beckmann CF, Adelstein JS, Buckner RL, Colcombe S, Dogonowski A-M, Ernst M, Fair D, Hampson M, Hoptman MJ, Hyde JS, Kiviniemi VJ, Kötter R, Li S-J, Lin C-P, Lowe MJ, Mackay C, Madden DJ, Madsen KH, Margulies DS, Mayberg HS, McMahon K, Monk CS, Mostofsky SH, Nagel BJ, Pekar JJ, Peltier SJ, Petersen SE, Riedl V, Rombouts SAR, Rypma B, Schlaggar BL, Schmidt S, Seidler RD, Siegle GJ, Sorg C, Teng G-J, Veijola J, Villringer A, Walter M, Wang L, Weng X-C, Whitfield-Gabrieli S, Williamson P, Windischberger C, Zang Y-F, Zhang H-Y, Castellanos FX, Milham MP. 2010. Toward discovery science of human brain function. *Proc Natl Acad Sci U S A* 107:4734–4739.
- Braga RM, Leech R. 2015. Echoes of the brain: local-scale representation of whole-brain functional networks within transmodal cortex. *Neuroscientist* [Epub ahead of print]; DOI: 10.1177/1073858415585730.
- Braga RM, Sharp DJ, Leeson C, Wise RJ, Leech R. 2013. Echoes of the brain within default mode, association, and heteromodal cortices. *J Neurosci* 33:14031–14039.
- Buckner RL, Krienen FM, Yeo BTT. 2013. Opportunities and limitations of intrinsic functional connectivity MRI. *Nat Neurosci* 16:832–837.
- Buckner RL, Sepulcre J, Talukdar T, Krienen FM, Liu HS, Hedden T, Andrews-Hanna JR, Sperling RA, Johnson KA. 2009. Cortical hubs revealed by intrinsic functional connectivity: mapping, assessment of stability, and relation to Alzheimer's disease. *J Neurosci* 29:1860–1873.
- Bullmore E, Sporns O. 2009. Complex brain networks: graph theoretical analysis of structural and functional systems. *Nat Rev Neurosci* 10:186–198.
- Calhoun VD, Adali T, Pearlson GD, Pekar JJ. 2001. A method for making group inferences from functional MRI data using independent component analysis. *Hum Brain Mapp* 14:140–151.
- Cole MW, Bassett DS, Power JD, Braver TS, Petersen SE. 2014. Intrinsic and task-evoked network architectures of the human brain. *Neuron* 83:238–251.
- Cole MW, Pathak S, Schneider W. 2010. Identifying the brain's most globally connected regions. *Neuroimage* 49:3132–3148.
- Cole MW, Reynolds JR, Power JD, Repovs G, Anticevic A, Braver TS. 2013. Multi-task connectivity reveals flexible hubs for adaptive task control. *Nat Neurosci* 16:1348–1355.
- Draganski B, Kherif F, Klöppel S, Cook PA, Alexander DC, Parker GJM, Deichmann R, Ashburner J, Frackowiak RSJ. 2008. Evidence for segregated and integrative connectivity patterns in the human basal ganglia. *J Neurosci* 28:7143–7152.
- Fox PT, Friston KJ. 2012. Distributed processing; distributed functions? *Neuroimage* 61:407–426.
- Geranmayeh F, Wise RJ, Mehta A, Leech R. 2014. Overlapping networks engaged during spoken language production and its cognitive control. *J Neurosci* 34:8728–8740.
- Haber S. 2008. Parallel and integrative processing through the Basal Ganglia reward circuit: lessons from addiction. *Biolo Psychiatry* 64:173–174.
- Hutchison RM, Womelsdorf T, Allen EA, Bandettini PA, Calhoun VD, Corbetta M, Della Penna S, Duyn JH, Glover GH, Gonzalez-Castillo J, Handwerker DA, Keilholz S, Kiviniemi V, Leopold DA, de Pasquale F, Sporns O, Walter M, Chang C. 2013. Dynamic functional connectivity: promise, issues, and interpretations. *Neuroimage* 80:360–378.

- Kalcher K, Huf W, Boubela RN, Filzmoser P, Pezawas L, Biswal BB, Kasper S, Moser E, Windischberger C. 2012. Fully exploratory network independent component analysis of the 1000 functional connectomes database. *Front Hum Neurosci* 6:301.
- Laird AR, Eickhoff SB, Rottschy C, Bzdok D, Ray KL, Fox PT. 2013. Networks of task co-activations. *Neuroimage* 80:505–514.
- Leech R, Kamourieh S, Beckmann CF, Sharp DJ. 2011. Fractionating the default mode network: distinct contributions of the ventral and dorsal posterior cingulate cortex to cognitive control. *J Neurosci* 31:3217–3224.
- Maldjian JA, Laurienti PJ, Kraft RA, Burdette JH. 2003. An automated method for neuroanatomic and cytoarchitectonic atlas-based interrogation of fMRI data sets. *Neuroimage* 19:1233–1239.
- Martuzzi R, Ramani R, Qiu M, Shen X, Papademetris X, Constable RT. 2011. A whole-brain voxel based measure of intrinsic connectivity contrast reveals local changes in tissue connectivity with anesthetic without a priori assumptions on thresholds or regions of interest. *Neuroimage* 58:1044–1050.
- Mesulam M. 1998. From sensation to cognition. *Brain* 121:1013–1052.
- Papo D, Zanin M, Pineda-Pardo JA, Boccaletti S, Buldú JM. 2014. Functional brain networks: great expectations, hard times and the big leap forward. *Philos Trans R Soc Lond B Biol Sci* 369:pii: 20130525
- Parvizi J. 2009. Corticocentric myopia: old bias in new cognitive sciences. *Trends Cogn Sci* 13:354–359.
- Power Jonathan D, Schlaggar Bradley L, Lessov-Schlaggar Christina N, Petersen Steven E. 2013. Evidence for hubs in human functional brain networks. *Neuron* 79:798–813.
- Sepulcre J, Liu HS, Talukdar T, Martincorena I, Yeo BTT, Buckner RL. 2010. The organization of local and distant functional connectivity in the human brain. *PLoS Comput Biol* 6:e1000808.
- Smith SM, Fox PT, Miller KL, Glahn DC, Fox PM, Mackay CE, Filippini N, Watkins KE, Toro R, Laird AR, Beckmann CF. 2009. Correspondence of the brain's functional architecture during activation and rest. *Proc Natl Acad Sci U S A* 106:13040–13045.
- Sporns O. 2011. *Networks of the Brain*. MIT Press, Cambridge.
- Sporns O. 2013. Network attributes for segregation and integration in the human brain. *Curr Opin Neurobiol* 23:162–171.
- Sporns O, Honey CJ, Kotter R. 2007. Identification and classification of hubs in brain networks. *PLoS One* 2:e1049.
- Tononi G, Sporns O, Edelman GM. 1994. A measure for brain complexity—relating functional segregation and integration in the nervous-system. *Proc Natl Acad Sci U S A* 91:5033–5037.
- van den Heuvel MP, Sporns O. 2013. An anatomical substrate for integration among functional networks in human cortex. *J Neurosci* 33:14489–14500.
- Van Essen DC, Drury HA, Dickson J, Harwell J, Hanlon D, Anderson CH. 2001. An integrated software suite for surface-based analyses of cerebral cortex. *J Am Med Inform Assoc* 8:443–459.
- Warren DE, Power JD, Bruss J, Denburg NL, Waldron EJ, Sun H, Petersen SE, Tranel D. 2014. Network measures predict neuropsychological outcome after brain injury. *Proc Natl Acad Sci U S A* 111:14247–14252.
- Yeo BT, Krienen FM, Chee MW, Buckner RL. 2013. Estimates of segregation and overlap of functional connectivity networks in the human cerebral cortex. *Neuroimage* 88C:212–227.
- Yeo BTT, Krienen FM, Sepulcre J, Sabuncu MR, Lashkari D, Hollinshead M, Roffman JL, Smoller JW, Zoller L, Polimeni JR, Fischl B, Liu HS, Buckner RL. 2011. The organization of the human cerebral cortex estimated by intrinsic functional connectivity. *J Neurophysiol* 106:1125–1165.
- Zalesky A, Breakspear M. 2015. Towards a statistical test for functional connectivity dynamics. *Neuroimage* 114:466–470.
- Zalesky A, Fornito A, Cocchi L, Gollo LL, Breakspear M. 2014. Time-resolved resting-state brain networks. *Proc Natl Acad Sci U S A* 111:10341–10346.
- Zuo X-N, Ehmke R, Mennes M, Imperati D, Castellanos FX, Sporns O, Milham MP. 2012. Network centrality in the human functional connectome. *Cereb Cortex* 22:1862–1875.

Address correspondence to:

*James M. Shine  
Brain and Mind Research Institute  
The University of Sydney  
94 Mallett Street  
Camperdown  
Sydney 2050  
New South Wales  
Australia*

*E-mail: mac.shine@sydney.edu.au*

**This article has been cited by:**

1. Peter T. Bell, James M. Shine. 2016. Subcortical Contributions to Large-Scale Network Communication. *Neuroscience & Biobehavioral Reviews* . [[CrossRef](#)]
2. Annabelle M. Belcher, Cecil Chern-Chyi Yen, Lucia Notardonato, Thomas J. Ross, Nora D. Volkow, Yihong Yang, Elliot A. Stein, Afonso C. Silva, Dardo Tomasi. 2016. Functional Connectivity Hubs and Networks in the Awake Marmoset Brain. *Frontiers in Integrative Neuroscience* **10**. . [[CrossRef](#)]